Research Article

Research on Energy Conversion and Damage Features of Unloading Instability of Sandstone under High Stress

Zhiyuan Hou [ID],[1] **Chuanbo Hao,**[2] **Fukun Xiao** [ID],[3] **and Gang Liu** [ID][3]

[1]*School of Safety Engineering, Heilongjiang University of Science and Technology, Harbin 150022, China*
[2]*Heilongjiang University of Science and Technology, Harbin 150022, China*
[3]*Heilongjiang Ground Pressure & Gas Control in Deep Mining Key Lab, Heilongjiang University of Science and Technology, Harbin 150022, China*

Correspondence should be addressed to Fukun Xiao; xiaofukun@hotmail.com

In order to explore the failure characteristics of sandstone under unloading conditions in deep zone with high stress, constant axial pressure and unloading confining pressure tests were conducted on a yellow sandstone sample under different initial confining pressures using the French ROCK600-50 triaxial tester, and the mechanical properties, energy conversion characteristics, and damage evolution law of sandstone failure under unloading conditions were obtained. The test results showed that the axial deformation, the confining pressure for failure, and the shear fracture energy during the failure process of sandstone under the unloading state were positively correlated with the initial confining pressure; the dilatancy amount and speed and the radial deformation were negatively correlated with the initial confining pressure, exhibiting the characteristics of dilatancy under low confining pressure and compression under high confining pressure. Before the unloading point, almost all the energy absorbed by the rock under low initial confining pressure was converted into elastic energy, while part of the energy absorbed under high initial confining pressure was converted into dissipated energy, and the higher the confining pressure, the greater the proportion of the dissipated energy converted. The higher the initial confining pressure, the greater the elastic energy, radial deformation energy, and dissipated energy at the rock fracture point. The larger the unloading confining pressure, the greater the postpeak failure energy and surplus energy of sandstone, and the greater the increase in the proportion of elastic energy converted into surplus energy. The higher the confining pressure, the larger the damage value at the unloading point; the damage speed in the unloading stage was significantly greater than that in the loading stage.

1. Introduction

With the gradual depletion of shallow mineral resources in recent years, deep mining is required. Therefore, it is necessary to excavate roadways and large chambers in the deep zone, and such excavation is actually a kind of unloading of the rock mass [1, 2]. The loading and unloading of the rock mass are two completely different stress states, with fundamentally different mechanical properties. Particularly, the mechanical changes caused by rock mass excavation and unloading in deep engineering are more complicated. Thus, studying the excavation unloading of the rock mass in the deep, high-stress zone is of great significance for understanding the

mechanical behavior and damage mechanism of deep rock mass under the unloading state.

Rock failure caused by the unloading conditions has attracted more and more attention from scholars at home and abroad, and a series of tests have been conducted. In terms of the study on the mechanical properties of rocks under unloading effect, Wang et al. [3] performed triaxial loading and unloading tests on deep-buried marbles and analyzed the failure behavior of marbles under different stress states from the perspective of mechanical parameters. Guo et al. [4, 5] explored the mechanical properties of rock failure under different unloading rates. Wen et al. [6, 7] carried out loading and unloading tests on rocks of Badong formation and quartz mica schist, and developed a

constitutive model based on the analysis of mechanical properties. Guo et al. [8] theoretically studied the evolution of the mechanical properties of the rock mass under the unloading state from the perspective of elastic strain energy. Li et al. [9, 10] conducted an unloading test on the rock mass containing joints, and discussed the impact of joint inclination angle on the mechanical properties of the rock sample. Regarding the research on rock deformation and dilatancy under the unloading effect, Yang et al. [11, 12] carried out the unloading test on transversely isotropic rock mass, and investigated the influence of parallel schistosity and vertical schistosity on the deformation and dilatancy of rock samples. Chen et al. [13] introduced the concept of dilatancy index to analyze the relationship between dilatancy index, dilatancy angle, and confining pressure. Hou et al. [14, 15] explored the deformation and damage characteristics of rock samples at different unloading rates. Xiao et al. [16–18] performed a true triaxial unloading test on sandstone under cyclic damage, and discussed the influence of the number of cyclic damages on the unloading failure characteristics of sandstone. In terms of the research on the unloading characteristics of rock under freezing-thawing and thermal damages, Yu et al. [19] studied the unloading of sandstone after freezing-thawing cycles, and examined the relationship between the number of freezing-thawing cycles and the mechanical parameters of rock samples. Ni et al. [20] analyzed the relationship between the number of freezing-thawing cycles and the damage degree of sandstone under unloading conditions. Cai et al. [21] investigated the unloading mechanical properties of granite under thermal damage. Chen et al. [22–24] studied the failure characteristics of the unloading of hard rock under thermal-mechanical coupling, and presented the relationship between rock mass temperature and rock burst intensity. In the study on energy evolution, Zhang et al. [25] carried out loading and unloading experiments on marble, respectively, focusing on the variation characteristics of each strain energy at the peak point. Fang et al. [26] analyzed the relationship between initial confining pressure and strain energy of a rock under unloading conditions. Li et al. [27] compared the evolution characteristics of the total strain energy, elastic strain energy, and dissipated energy of a hard rock under loading and unloading stress.

The above research results are of great significance for the analysis of the mechanical properties, deformation characteristics, and energy evolution characteristics of the rock under the unloading conditions. However, most scholars adopted the loading method of increasing axial pressure and unloading confining pressure, while in the excavation of roadway, the rock mass close to the sidewall of the roadway is actually approximately in the stress state of constant axial pressure and unloading confining pressure. At the same time, the analysis of the dissipated energy in the above research results runs through the entire test, and the energy released after rock failure includes part of the kinetic energy. It is common to analyze the energy conversion after failure using the dissipated energy alone. Based on this, it is necessary to carry out experimental research on the constant axial pressure and the unloading confining pressure of

sandstone under high stress, so as to explore the failure characteristics of sandstone under different initial confining pressures from the perspectives of mechanical properties, energy conversion before failure, energy release after failure, and damage evolution.

2. Test Method and Principle

2.1. Preparation of Test Sample. Yellow sandstone was selected as the test material, and the SC-200 rock sample core-drilling machine was used to drill the rock cores with a diameter of 50 mm along the vertical bedding direction according to the methods for determining the triaxial strength and the deformation parameters of coal and rock (GB/T 23561.9–2009). The rock cores were processed into standard $\varphi 50 \times 100$ mm rock samples with the non-parallelism of both end faces being less than 0.05 mm. Then, they were placed in a drying box for 24 hours at a temperature of 120°. The Sonic Viewer-SX rock sample ultrasonic system was used for screening, and the sample with the P-wave velocity of roughly 3900 m/s, and the S-wave velocity of about 3100 m/s was selected to reduce the dispersion of the sample. The prepared sample is shown in Figure 1.

2.2. Test System. The loading device in the test is equipped with the TOP INDUSTRIE Rock 600–50 full-automatic servo rheometer. It is composed of axial pressure, confining pressure, and seepage pressure servo devices. The system can apply a maximum axial stress of 375 MPa, a maximum confining pressure of 60 MPa, and a maximum pore fluid pressure of 50 MPa, with a pressure control accuracy of 0.01 MPa. Two linear displacement sensors (LVDT) are used to collect the axial strain, and the hoop strain is collected using the hoop electronic strain gauge placed in the center of the rock sample. The collection accuracy of sample deformation can reach the micron level. The test system is shown in Figure 2.

2.3. Test Scheme and Principle. In order to simulate the stress state of the two sidewalls in the roadway excavation process, this test adopted the loading methods of constant axial pressure (σ_1) and unloading confining pressure (σ_3). The stress path is displayed in Figure 3(a). According to the different mining depths, the confining pressure was set to 10 MPa, 20 MPa, 30 MPa and, 40 MPa; pressure over 20 MPa can generally be defined as high stress. The axial pressure was set to 70% of the limit load of the rock sample in the conventional triaxial test under different confining pressure conditions. During the test, the rock sample was placed into the pressure chamber and loaded to the predetermined confining pressure at a speed of 2 MPa/min. After the confining pressure was stable for 5 minutes, the axial pressure was loaded to the predetermined value at a speed of 2 MPa/min, and was maintained as stable for 5 minutes, after which the axial pressure was kept constant while the confining pressure was unloaded at the rate of 0.9 MPa/min until the failure of the rock sample. The initial stress state of the rock sample is shown in Table 1.
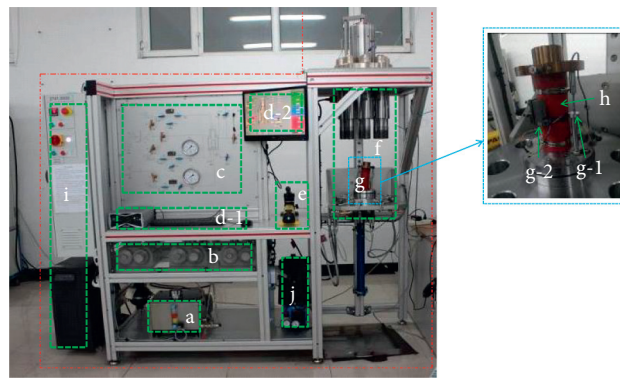
FIGURE 1: Yellow sandstone samples.

FIGURE 2: Experimental system of rock mechanics. (a) oil source; (b) axis, enclosure, and pore water loading pump; (c) monitoring and control panels; (d): computer acquisition control system d-1, control system display and d-2, and the host of the control system; (e) base lift pump; (f) Experimental cylinder block; (g) base (g-1: axial sensor; g-2: circumferential sensor); (h) rock sample; (i) power; and (j) pressure pump for confining pressure room.
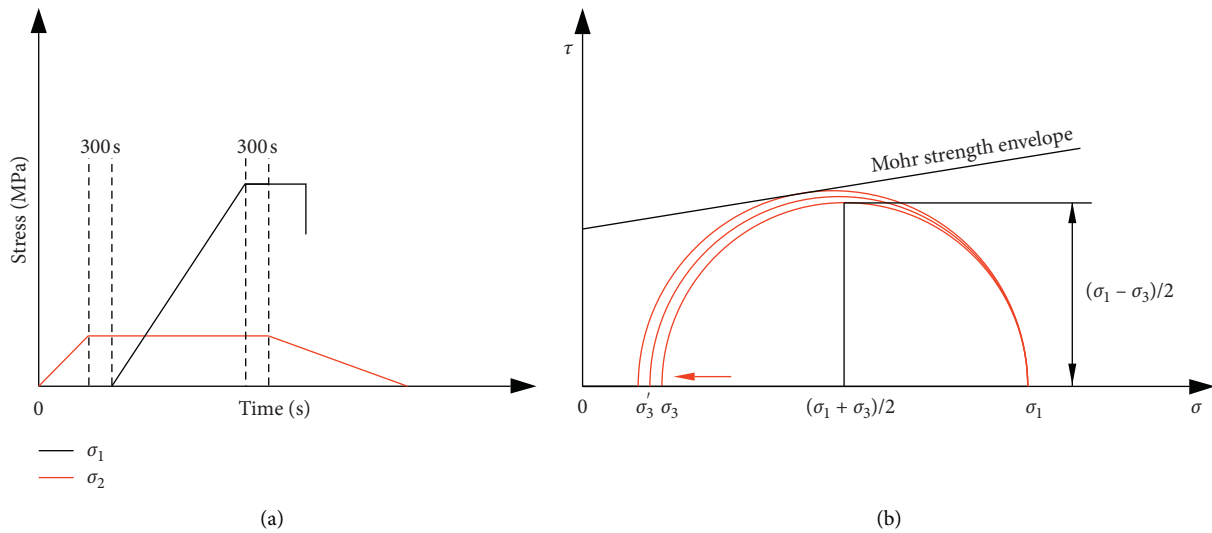

| (a) | (b) |

FIGURE 3: Experimental process of sandstone unloading. (a) Experimental stress path (b) Failure principle of rock samples.

According to the Mohr–Coulomb criterion, there exists a resultant force on the plane of every tiny element inside the rock, which can be decomposed into normal stress (σ) and shear stress (τ). Each group of normal stress (σ) and shear stress (τ) are distributed on a circular arc with $((\sigma_1 + \sigma_3/2),\ 0)$ as the center and a radius of $(\sigma_1 - \sigma_3/2)$ [28]. As shown in

TABLE 1: Initial stress state of rock samples.

Specimen ID	σ_3 (MPa)	Loading rate (MPa/min)	σ_1 (MPa)	Loading rate (MPa/min)	Unloading rate (MPa/min)
10-a, 10-b, 10-c, 10-d, 10-e	10		105		
20-a, 20-b, 20-c, 20-d, 20-e	20		144		
30-a, 30-b, 30-c, 30-d, 30-e	30	2	188	2	0.9
40-a, 40-b, 40-c, 40-d, 40-e	40		225		

Figure 3(b), when σ_3 continuously decreases, the center of the circle continues to move to the left, and the radius of the arc constantly increases until the arc is tangent to the strength envelope, after which the small units inside the rock sample show shear slip until the failure of the rock sample.

3. Analysis of Mechanical Characteristics of Sandstone Failure under Unloading Conditions

3.1. Deformation Characteristics of Sandstone under Unloading Conditions. The test results were analyzed and calculated, and the typical stress-strain curves of the yellow sandstone under confining pressures of 10 MPa, 20 MPa, 30 MPa, and 40 MPa were obtained, as shown in Figure 4 (σ_1 is the axial stress, σ_3 is the hoop stress, $\sigma_1-\sigma_3$ is the deviator stress on the sample, ε_1 is the axial strain, and ε_3 is the radial strain). The slight concavity of the stress-strain curve at the initial loading of the sample indicates that the particles inside the sample are compacted. The stress-strain curve at the loading stage to the unloading point is almost a straight line, and the slope of the curve at the loading stage under different confining pressures is basically the same. The rock sample shows good linear elasticity, and has no obvious yield phenomenon compared with the rock sample at the loading stage in the conventional triaxial test. During the stage of unloading, confining pressure σ_3 keeps decreasing. Although $\sigma_1-\sigma_3$ remains basically unchanged, the axial strain ε_1 continuously increases. As the confining pressure reduces, the rock sample exhibits prominent characteristics of axial plastic flow, so that the load capacity of rock sample gradually decreases, and the deviator stress $\sigma_1-\sigma_3$ slightly drops. It can be seen from the change in the slope of the stress-strain curves after the fracture point of the rock sample that the slope of the curve under high confining pressure is obviously greater than the slope under low confining pressure, suggesting that the instability failure point of the rock sample falls to the residual strength point at an obviously larger speed under high confining pressure unloading than that under low confining pressure; in addition, during the test, the rock sample failed under high confining pressure unloading and made a clear and crisp sound, indicating that the failure of the rock sample under high confining pressure unloading shows an obvious brittle fracture, which means that under the condition of deep high-stress excavation and unloading, the instability failure of the rock mass is dominated by brittle failure, with obvious suddenness.
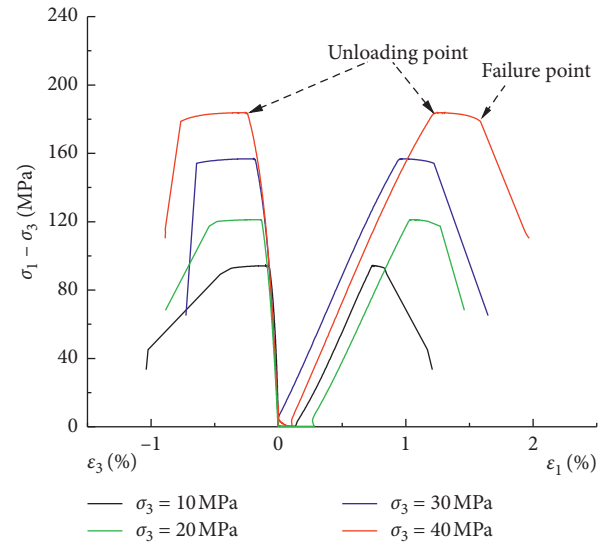

FIGURE 4: Typical stress-strain curve of sandstone under unloading condition.

Figure 5 displays the variation curve of volume strain (ε_v) of the yellow sandstone failure under unloading conditions with different confining pressures, where the curve rise represents volume compression, and the curve decline represents volume expansion. The positive value of the volume strain at the residual stress point indicates that the failed rock sample is finally compressed, and the negative value of the volume strain at the residual stress point indicates that the failed rock sample is ultimately dilated. The failure of sandstone under different confining pressures shows volume compression and then dilatancy. The volume compression mainly occurs in the initial stress stage and the initial stage of unloading confining pressure. After reaching the damage dilatancy point, the rock sample presents obvious dilatancy. The main reason for this phenomenon is that as the confining pressure $\sigma3$ is continuously reduced, the stress Mohr's circle gradually moves to the left, with the radius increasing, gradually approaching the strength envelope, causing the development and expansion of the internal cracks of the rock sample, which coupled with the continuous reduction of lateral constraints leaves the rock sample significantly dilated. From the changes in the dilatancy point of the rock sample in the figure, it can be found that the larger the confining pressure, the greater the axial strain required by the dilatancy point, which also means that
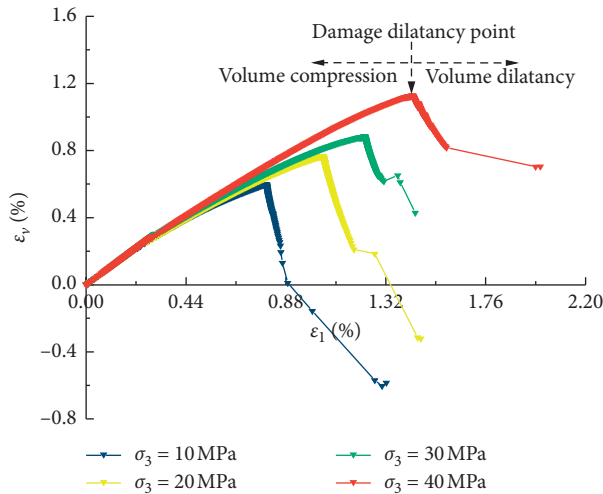
FIGURE 5: Axial strain-volume strain curve of sandstone under the unloading condition.

high confining pressure plays a certain role in suppressing the dilatancy characteristics of the rock sample failure. In the figure, when the confining pressures are 10 MPa, 20 MPa, 30 MPa, and 40 MPa, the volume strain (ε_v) at the residual stress points are −0.584%, −0.321%, 0.610%, and 0.705%, respectively, suggesting that with the continuous increase of the confining pressure, the final failure of the rock sample gradually changes from dilatancy to compression, which is manifested in the dilatancy failure under low confining pressure and compression failure of the rock sample under high confining pressure. By observing the dilatancy deformation amount of the rock sample after the damage dilatancy point under different confining pressures and the slope of the dilatancy curve, it can be found that with the continuous increase of confining pressure, the dilatancy amount and speed of the rock sample show a decreasing trend, demonstrating that the ductility characteristics of the failure of the rock sample under unloading conditions weaken with the increase of confining pressure, while the brittleness characteristics continue to strengthen with the increasing confining pressure.

Figure 6 shows the typical curves of the relationship between axial strain (ε_1), radial strain (ε_3), volume strain (ε_v) and confining pressure (σ_3) under different confining pressures. It can be seen from the figure that in the initial stage of unloading confining pressure, axial strain, radial strain, and volume strain all increase slowly with the decrease of confining pressure, showing a linear variation, indicating that the rock sample exhibits elastic changes at the initial stage of unloading; approaching the inflection point of the curve, the three kinds of strain nonlinearly change with the confining pressure, and the rock sample shows obvious characteristics of plastic changes; at the inflection point of the curve, as the confining pressure continues to reduce, all three kinds of strain have a sudden increase. At this time, the internal cracks of the rock sample rapidly develop and penetrate to form macroscopic cracks, demonstrating that the failure of the rock under unloading conditions also needs to experience elastic deformation stage,
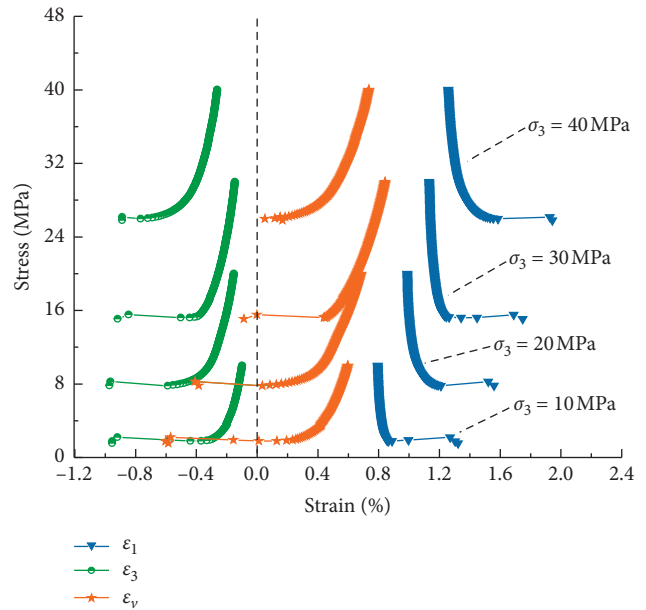

FIGURE 6: Relationship curve of confining pressure, axial strain, radial strain, and volume strain of sandstone under the unloading condition.

plastic deformation stage, and yield stage. Through the change law of axial strain (ε_1), it can be found that from the low confining pressure unloading ($\sigma_3 = 10$ MPa) to the inflection point, the axial deformation is small; with the continuous increase of the confining pressure, the axial strain also increases before the unloading reaches the critical point of failure, indicating that the axial deformation of the rock sample under high stress unloading is significantly greater than that under low stress. The calculated proportions of radial deformation in the axial deformation in the entire unloading process are 161.93% ($\sigma_3 = 10$ MPa), 143.50% ($\sigma_3 = 20$ MPa), 125.47% ($\sigma_3 = 30$ MPa), and 91.40% ($\sigma_3 = 40$ MPa), respectively; it can be seen that the radial deformation of the rock sample gradually decreases with the increase of confining pressure, and the radial deformation of the failure of the rock sample under low confining pressure is obviously greater than that under high confining pressure. This is mainly because the reduction of the confining pressure is actually equivalent to a hoop tensile stress, which then produces cracks parallel to the axial direction, so that the radial deformation under the unloading conditions is significantly greater than the axial deformation. Under high confining pressure, the confining pressure exerts an inhibitory effect on the crack expansion caused by the hoop tensile stress; thus, the radial deformation drops as the confining pressure increases.

Figure 7 presents the relationship between the initial confining pressure and the failure confining pressure during the failure process of the rock sample under the condition of unloading confining pressure. It can be found from the figure that the confining pressure for the failure of the rock sample under unloading conditions increases with the increasing initial confining pressure, exhibiting a good linear relationship. The relationship between the two after data fitting is shown in
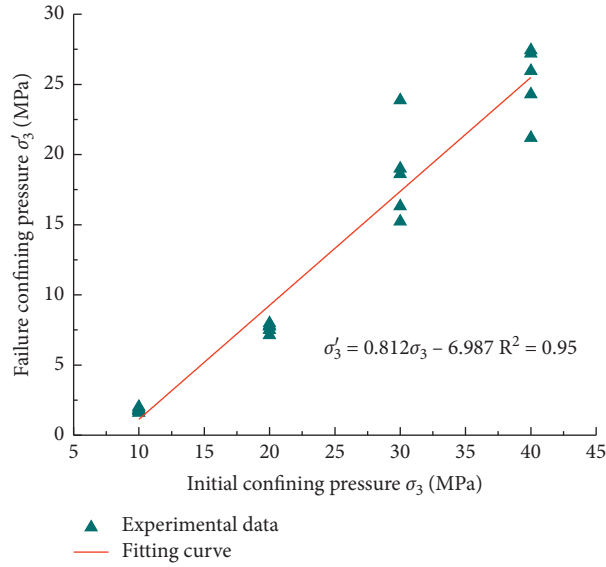
FIGURE 7: Relationship between initial confining pressure and failure confining pressure.

$$\sigma_3' = 0.812\sigma_3 - 6.987 R^2 = 0.95, \qquad (1)$$

where σ_3 is the initial confining pressure, and σ_3' is the failure confining pressure.

3.2. Variation Characteristics of the Shear Fracture Energy of Sandstone under Unloading Conditions with Different Confining Pressures. Before the shear failure of the rock sample,

a deformation concentration zone will be formed along the shear surface (see Figure 8(a). In this zone, the energy absorbed by per unit area of the shear zone due to deformation is the shear fracture energy. Therefore, the failure of the rock sample can be considered as a slip along the shear surface at the macro level. The shear fracture energy (G) before the failure of the rock sample can be calculated by [29]

$$G = L\left[\int_0^{\varepsilon_P} (\sigma_1 - \sigma_3)\mathrm{d}\varepsilon_1 - \frac{\sigma_p}{2E}\right] = L\left[\sum_{i=1}^{i=i_p} \frac{1}{2}\left(\sigma_{11}^i + \sigma_{11}^{i+1} - \sigma_{31}^i - \sigma_{31}^{i+1}\right)\left(\varepsilon_{11}^{i+1} - \varepsilon_{11}^i\right) - \frac{\sigma_p}{2E}\right], \qquad (2)$$

where G is the shear fracture energy; L is the length of the sample; σ_p is the peak stress; ε_p is the strain corresponding to the peak stress; and E is the initial elastic modulus.

Table 2 provides the shear fracture energy required for the failure of the yellow sandstone sample under unloading conditions with different confining pressures calculated by the above formula. The shear fracture energies are 27.75 N/mm ($\sigma_3 = 10$ MPa), 48.28 N/mm ($\sigma_3 = 20$ MPa), 77.02 N/mm ($\sigma_3 = 30$ MPa), and 111.78 N/mm ($\sigma_3 = 40$ MPa), respectively. This shows that the shear fracture energy required for the failure of the sandstone sample under unloading conditions increases with the increase of the confining pressure, and the larger the confining pressure, the greater the increase of the shear fracture energy required. In the test of unloading confining pressure, as the confining pressure continuously reduces, the shear fracture energy required for sample failure also continuously drops, and when the shear fracture energy on the shear surface is just equal to the shear fracture energy required for the failure of the sample, the sandstone sample is damaged. In the excavation of deep roadways, the reduction of the confining pressure of the rock mass should be

controlled as much as possible to improve the stability of the roadways. The shear fracture energies required for the failure of sandstone under unloading conditions with different confining pressures were fitted, as shown in Figure 8(b). It can be seen that there is a quadratic polynomial positive correlation fitting relationship between the shear fracture energy and the confining pressure, as displayed in

$$G = 0.036\sigma_3^2 + 1.029\sigma_3 + 13.794 R^2 = 0.98, \qquad (3)$$

where G is the shear fracture energy, and σ_3 is the confining pressure.

4. Analysis on Energy Conversion of Sandstone under Unloading Conditions

4.1. Principle of Energy Calculation. From the perspective of energy, it is considered that the process wherein a rock is loaded to failure is essentially the process of energy input, accumulation, dissipation, and release. Without considering the heat exchange with the outside world, part of the work done

TABLE 2: Shear fracture energy of rock samples under different confining pressures.

Specimen ID	σ_3 (MPa)	E (GPa)	L (mm)	G (N/mm)	Average (N/mm)
10-a		16.48	100.06	25.54	
10-b		16.67	100.69	28.25	
10-c	10	16.71	99.74	29.98	27.75
10-d		16.82	100.19	27.97	
10-e		16.95	100.18	27.00	
20-a		16.43	100.07	46.80	
20-b		16.58	100.18	47.22	
20-c	20	16.57	100.02	48.23	48.28
20-d		16.22	100.92	49.18	
20-e		16.63	100.21	49.97	
30-a		18.11	100.18	75.05	
30-b		18.78	99.13	71.48	
30-c	30	16.50	101.25	82.53	77.02
30-d		17.37	100.94	79.24	
30-e		17.49	100.16	76.78	
40-a		17.47	100.18	110.11	
40-b		16.89	99.76	116.53	
40-c	40	17.61	100.86	115.00	111.78
40-d		19.30	100.12	96.58	
40-e		16.92	100.51	120.68	

(a)

$$G = 0.036\sigma_3^2 + 1.029\sigma_3 + 13.794$$
$$R^2 = 0.98$$
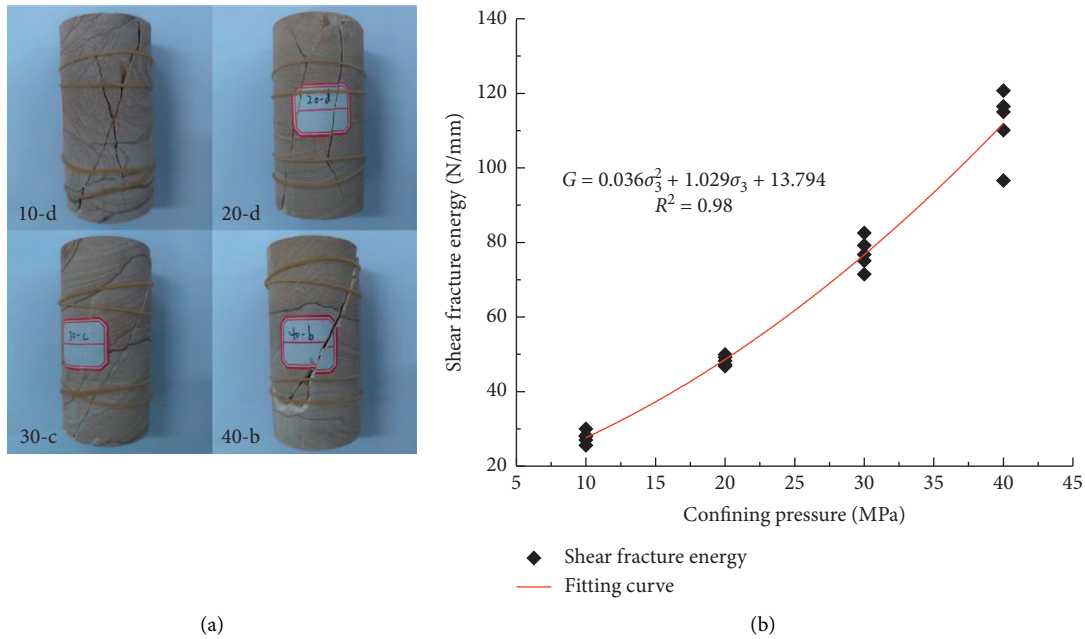
◆ Shear fracture energy
— Fitting curve

(b)

FIGURE 8: Failure of rock samples. (a) Failure diagram of rock samples under different confining pressures. (b) Shear fracture energy of rock samples under different confining pressures.

by the external force on the rock will be stored in the rock in the form of elastic strain energy, and the other part will be dissipated in the form of dissipated energy. When the elastic energy accumulated by the rock exceeds its bearing limit, it will suddenly break and release the stored elastic energy [30].

In the triaxial unloading confining pressure test, the stress, deformation, and failure of the sample are all carried out in the hydraulic cylinder. The sample and the testing machine can be regarded as a closed system. Without considering the heat exchange between the system and the outside, the work done by the test machine will all be stored in the rock, that is, the total energy U, including the positive work U_1 done by the axial stress, the positive work U_0 done by the hydrostatic pressure, and the negative work U_3 (overcoming the loop deformation of the rock) done by the confining pressure, as shown in

$$U = U_1 + U_3 + U_0. \tag{4}$$

During the test, the positive work (U_1) done by the axial stress and the negative work (U_3) done by the confining pressure on the rock sample can be obtained from the stress-strain curve, and its physical meaning is the area enclosed by the stress-strain curve. The calculation method is shown in [31]

$$\begin{cases} U_1 = \int_0^{\varepsilon_1^t} \sigma_1 d\varepsilon_1, \\ U_3 = 2 \int_0^{\varepsilon_3^t} \sigma_3 d\varepsilon_3, \end{cases} \tag{5}$$

where ε_3^t is the axial strain of the rock sample at time t, σ_1 is the axial stress at time t; ε_3^t is the radial strain at time t, and σ_3 is the radial stress at time t.

The work done by the hydrostatic pressure (U_0) can be regarded as a constant value, and this part of the energy is the elastic energy stored in the rock sample that can be completely released. It can be directly obtained by the theory of elasticity mechanics, as shown in [32]

$$U_0 = \frac{3(1 - 2\overline{v})}{2\overline{E}} (\sigma_3^0)^2, \tag{6}$$

where σ_3^0 is the hydrostatic pressure value of the rock sample, $\overline{E}$ is the average unloading elasticity modulus, and $\overline{v}$ is the average unloading Poisson's ratio. Generally, the elastic modulus E_0 and Poisson's ratio v of the initial loading stage are used.

The total energy U input by the test machine will be transformed into two parts in the rock sample. One part is the elastic energy U_e stored in the rock, and the other part is the dissipated energy U_d for internal damage and plastic deformation of the rock. The relationship is displayed in Formula (7). The elastic energy stored inside the rock during the loading of the rock can be calculated by Formula (8), and the dissipated energy can be calculated by Formula (9) [33]:

$$U = U_e + U_d, \tag{7}$$

$$U_e = \frac{1}{2\overline{E}} \left[\sigma_1^2 + 2\sigma_3^2 - 2\overline{v}(2\sigma_1\sigma_3 + \sigma_3^2) \right], \tag{8}$$

$$U_d = U_1 + U_3 + U_0 - U_e, \tag{9}$$

where $\overline{E}$ is the average unloading modulus, $\overline{v}$ is the average unloading Poisson's ratio, which can be replaced by the initial elastic modulus E_0 and Poisson's ratio v.

During the loading process of the rock, with the internal damage, the elastic energy stored will exceed its bearing limit and be released suddenly, leading to instantaneous failure of the rock. Part of the released elastic energy is used for the fracture of the rock, that is, the postpeak failure energy U_f, which is calculated by Formula (10); the other part is the surplus energy U_y, which is mainly the initial kinetic energy used for rock failure ejection. The calculation method is shown in Formula (11) [34]. The relationship between the total input U, the stored elastic energy U, the dissipated

energy U_d, the postpeak failure energy U_f, and the surplus energy U_y from the rock loading to failure is shown in Figure 9.

$$U_f = \int_{\varepsilon_f}^{\varepsilon_{\max}} \frac{\sigma_i + \sigma_{i+1}}{2} d\varepsilon, \tag{10}$$

$$U_y = U_e - U_f, \tag{11}$$

where ε_f is the strain at the failure point of the rock sample, $\varepsilon_{\max}$ is the strain at the residual stress point of the rock sample, and σ_i is the stress at the segmented point.

4.2. Analysis of Energy Conversion in the Failure of Sandstone under Unloading Conditions. According to the energy calculation method in the previous section, combining the test data, the energy conversion characteristics of the failure process of the yellow sandstone sample under unloading conditions with different initial confining pressures were calculated, as exhibited in Figure 10 and Table 3. Figure 10 shows that the overall change trend of the total energy (U), elastic energy (U_e), dissipated energy (U_d), and radial strain energy (U_3) inside the rock during the process wherein the sandstone sample is loaded to the failure under unloading confining pressure is similar. In the initial stage of loading, U, U_e, and U_d all rise with an increase in stress. At the initial stage of loading, the compaction of micro particles and the closure of micro cracks consume part of the energy, so the dissipated energy increases gradually. After the unloading point, the total energy and the dissipated energy inside the rock reduce first and then increase. The reason is that the sudden decrease in the confining pressure causes a sudden increase of the radial deformation of the rock sample, which results in the sudden rise of the radial strain energy doing negative work, thereby reducing the total energy inside the sample. As the press machine continues to work on the rock, the total energy inside the sample increases constantly again. In the whole process of unloading the confining pressure, the elastic energy inside the rock remains almost unchanged, and this is the reason why the dissipated energy decreases first and then increases. This also means that the total energy input by the press machine during the whole stage of unloading the confining pressure is almost completely converted into the dissipated energy inside the rock, which is used for the development and expansion of micro-cracks until the rock loses its bearing capacity and fails.

However, the difference is that before the unloading point, U and U_e under low initial confining pressure ($\sigma_3 = 10$ MPa) are almost parallel, and gradually separate as the initial confining pressure increases, and when the initial confining pressure is 40 MPa, the distance between the two is the largest. This indicates that almost all the energy absorbed by the rock under low initial confining pressure is converted into elastic energy before the unloading point, while most of the energy absorbed under high initial confining pressure is converted into elastic energy, and a small part is converted into dissipated energy. At the same time, it also means that there is almost no damage inside the rock under low confining
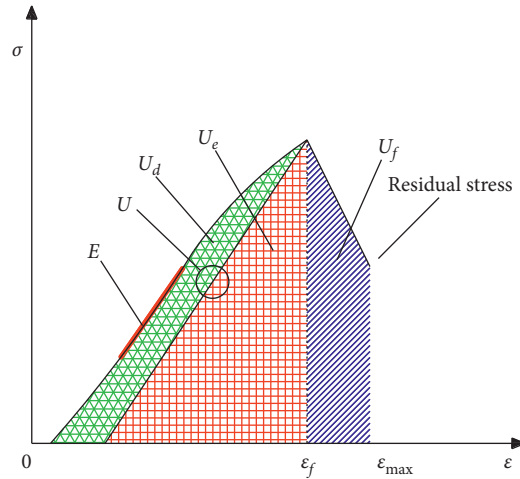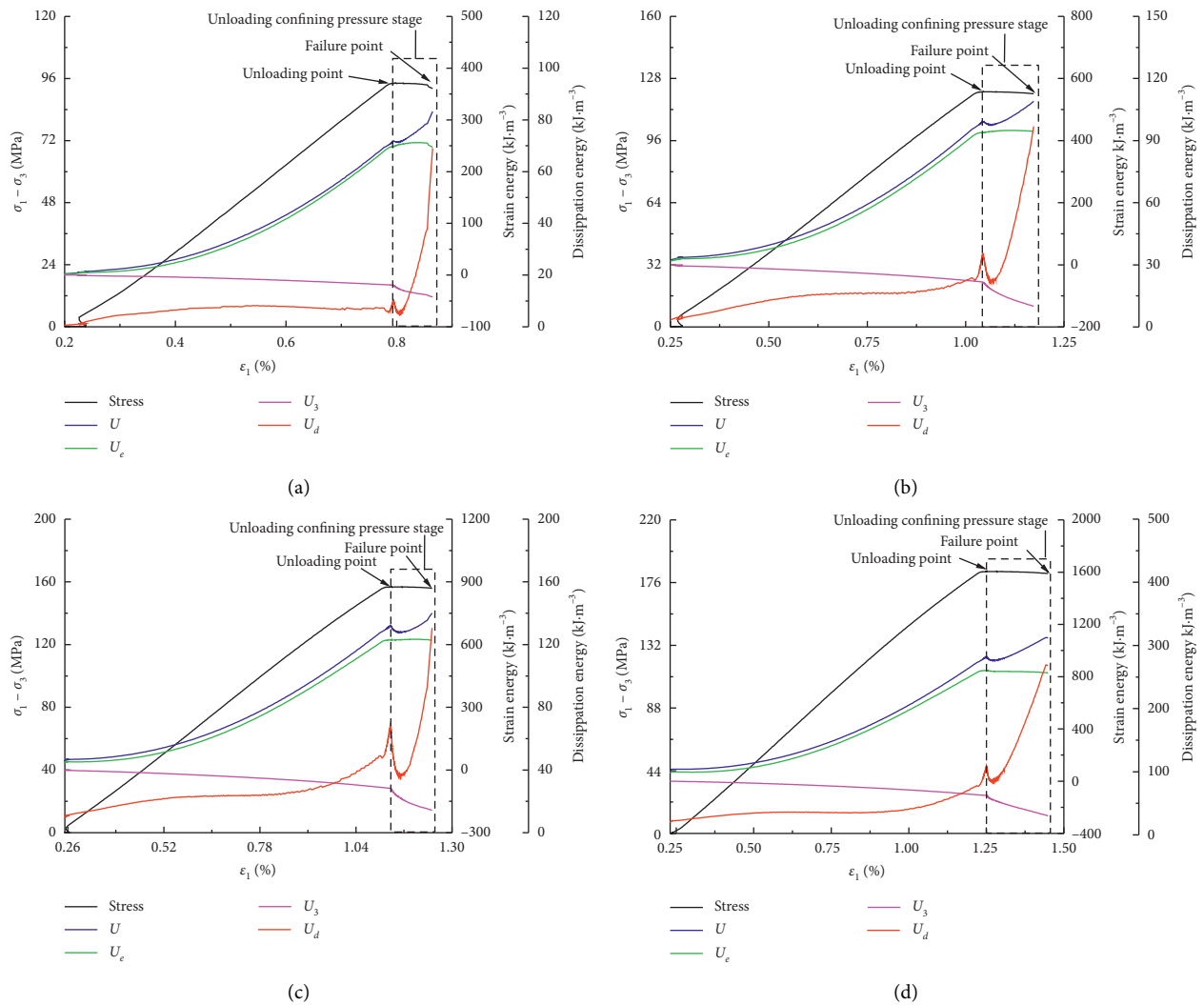
FIGURE 9: Energy conversion relationship.

FIGURE 10: Energy transformation diagram of sandstone unloading failure under different initial confining pressures. (a) 10-e, (b) 20-d, (c) 30-b, and (d) 40-d.

TABLE 3: Energy transformation of sandstone unloading failure under different initial confining pressures.

Initial confining pressure (MPa)	U (kJ·m^{-3})	U_3 (kJ·m^{-3})	U_e (kJ·m^{-3})	U_d (kJ·m^{-3})	U_f (kJ·m^{-3})	U_y (kJ·m^{-3})
10	342.36	−43.59	243.54	98.82	229.01	14.52
20	572.60	−138.76	409.73	162.87	318.50	91.23
30	899.73	−205.33	632.76	266.97	458.16	174.60
40	1246.37	−383.10	898.08	348.29	558.46	339.61

Note. Data are average values, and curve is a typical curve.

pressure before the unloading point, while there is a certain degree of damage of the rock under high confining pressure before the unloading point. This feature can also be found through the change in the dissipated energy (U_d). The dissipated energy under each confining pressure in the early stage of loading increases, which is mainly attributed to the compaction of rock particles and the closure of micro-cracks, and before loading to the unloading point, the dissipated energy under low confining pressure ($\sigma_3 = 10$ MPa) remains almost unchanged, but increases under high confining pressure. It can be found from Table 3 that the conversion amount of each energy index at the rock fracture point increases with the increasing initial unloading confining pressure. Due to the increase in the confining pressure in the loading stage, the bearing limit and axial strain of the rock also increase, thus the total energy absorbed and the stored elastic energy also increase with the rise in the confining pressure. When the confining pressure increases from 10 MPa to 40 MPa by an increase of 10 MPa, the total energy (U) under different confining pressures is 1.51, 2.63, and 3.64 times the total energy under the confining pressure of 10 MPa, and the elastic energy (U_e) is 1.68, 2.60, and 3.69 times larger, respectively. The radial strain energy is the accumulation of the energy consumed for doing work to overcome the confining pressure in the process of the increase in the radial deformation of the rock. The higher the initial unloading confining pressure, the greater the resistance for the radial deformation of the rock and the larger the energy consumed. When the confining pressure increases from 10 MPa to 40 MPa by an increase of 10 MPa, the radial strain energy (U_3) under different confining pressures is 3.18, 4.71, and 8.79 times larger than that under the confining pressure of 10 MPa, and the dissipated energy (U_d) is 1.65, 2.70, and 3.52 times greater, respectively.

4.3. Analysis of the Variation Characteristics of Dissipated Energy during the Unloading Process. Figure 11(a) shows the variation characteristics of the dissipated energy (U_d) during the unloading process under different initial confining pressures. It can be seen from the figure that the higher the initial confining pressure, the greater the dissipated energy required for the failure of the rock sample under unloading conditions, and there is a positive correlation. By observing the characteristics of the changes in the curve of dissipated energy before the unloading point, it can be found that the higher the initial confining pressure, the greater the increase of the dissipated energy curve; at the same time, the

dissipated energy value at the unloading point is also larger. Since the dissipated energy in the process of rock failure is mainly used for the development and expansion of internal cracks [35], the larger the dissipated energy, the greater the degree of damage of the rock sample, and the greater the damage of the rock sample under higher initial confining pressure before unloading.

In order to better analyze the role of dissipated energy in the entire failure process of the rock, the evaluation index, the ratio of dissipated energy (U_d/U) [27, 36] was introduced, as shown in Figure 11(b). It can be seen from the figure that in the initial compaction stage, the lower the confining pressure, the higher the proportion of dissipated energy, indicating that the smaller the confining pressure, the greater the proportion of energy consumed by the compaction of the particles of the rock sample and the closure of micro-cracks. The main reason is the influence of hydrostatic pressure. The higher the hydrostatic pressure, the greater the compression of the rock sample; therefore, the required dissipated energy in the compaction stage is small when the axial stress increases. The observation of the variation characteristics of the curve of the dissipated energy ratio before the unloading point in the figure reveals that the curve shows a downward trend under low confining pressure ($\sigma_3 = 10$ MPa), indicating that the proportion of the dissipated energy before the unloading of the rock sample under low confining pressure is gradually decreasing. As the confining pressure continues to rise, the curve gradually exhibits a decrease and then an increase, and the higher the confining pressure, the more obvious the trend, suggesting that the proportion of the dissipated energy before the unloading of the rock sample increases with the increasing initial confining pressure; at the same time, the higher the confining pressure, the greater the proportion of dissipated energy at the unloading point. The above change characteristics of the curve also indirectly demonstrate that the higher the initial confining pressure, the greater the degree of damage of the rock sample before unloading. Therefore, the damage degree of the rock mass before excavation under high stress is greater than that under low stress.

4.4. Analysis of Characteristics of Energy Release after Failure under Unloading Conditions. Figure 12 displays the relationship between the postpeak failure energy (U_f), surplus energy (U_y), and confining pressure after the failure of the yellow sandstone under unloading conditions with different initial confining pressures. It can be seen from Figure 12(a) that the elastic energy, postpeak failure energy, and surplus energy inside the rock all increase
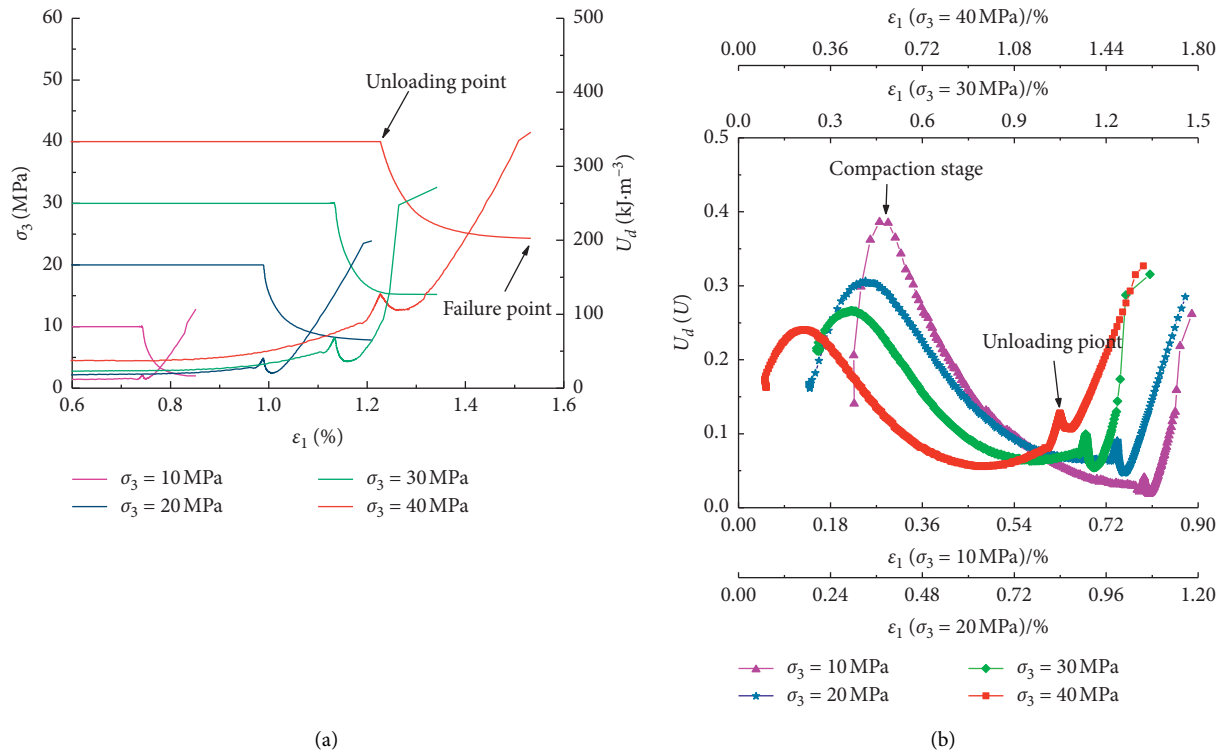
(a)

(b)

FIGURE 11: Typical curves of dissipation energy variation of sandstone unloading failure under different initial confining pressures. (a) Relationship between confining pressure and dissipative energy. (b) Evolution characteristics of (U)d/(U) under different initial confining pressures.
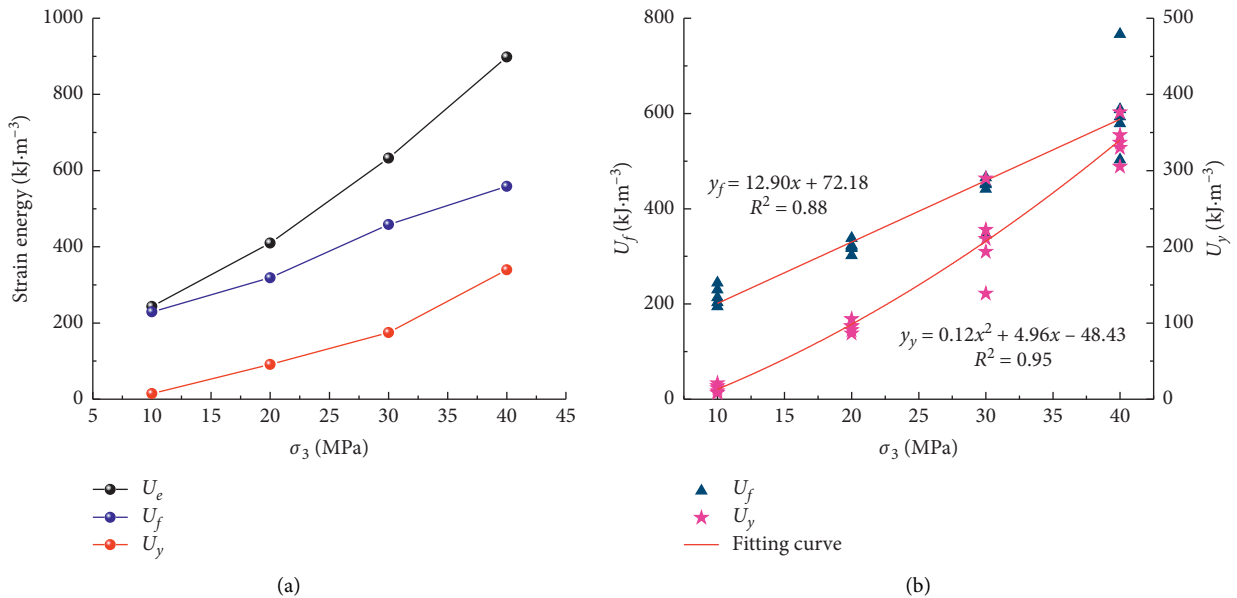

(a)

(b)

FIGURE 12: Energy variation characteristics of sandstone after unloading failure. (a) Energy transformation of sandstone after unloading failure under different initial confining pressure. (b) Fitting of postpeak failure energy, surplus energies and the initial confining pressure.

with the increase of the confining pressure, indicating that the higher the confining pressure, the greater the energy that acts on the cracks during the rock failure, and the more complete the rock failure. This also means that the rock failure under unloading conditions in the deep high-

stress zone is greater than that in the shallow zone. Since the energy of rock failure mainly comes from the release of internal stored elastic energy [37], the postpeak failure energy of the rock is converted from the stored elastic energy, while the remaining surplus energy is used as the

initial kinetic energy for the ejection of rock fragments, showing the dynamic phenomenon of failure. It can be observed from the figure that under low confining pressure ($\sigma_3 = 10$ MPa), almost all of the elastic energy inside the rock is converted into postpeak failure energy, and the surplus energy is at an extremely low level, and there is no obvious brittle fracture sound when the rock fails. With the continuous increase of the initial confining pressure, the curve of elastic energy and the curve of postpeak failure energy gradually separate, and the proportion of elastic energy converted into postpeak failure energy gradually reduces, reaching 77.73% ($\sigma_3 = 20$ MPa), 72.41% ($\sigma_3 = 30$ MPa), and 62.18% ($\sigma_3 = 40$ MPa), respectively, which means that a higher proportion of elastic energy is converted into surplus energy. As shown in Figure 12(a), as the initial confining pressure continues to rise, the surplus energy presents a parabolic increasing trend. When the confining pressure increases from 10 MPa to 40 MPa by an increase of 10 MPa, the surplus energies (U_y) under different confining pressures is 6.28, 12.02, and 23.39 times larger than that under the confining pressure of 10 MPa, respectively. It can be seen that every time the initial confining pressure doubles, the surplus energy during unloading failure increases several times, which indirectly indicates that the rock failure during deep high-stress excavation unloading will be accompanied by a large amount of surplus energy, resulting in mine dynamic disasters such as rock burst.

Figure 12(b) shows the fitting relationship between postpeak failure energy (U_f), surplus energy (U_y), and confining pressure under different initial confining pressures. There is a good linear relationship between postpeak failure energy and confining pressure, and there is a good quadratic polynomial relationship between surplus energy and confining pressure, as shown in Formula (12) and Formula (13), respectively.

$$y_f = 12.90x + 72.18 R^2 = 0.88, \tag{12}$$

$$y_y = 0.12x^2 + 4.96x - 48.43 R^2 = 0.95, \tag{13}$$

where y_f is the postpeak failure energy, y_y is the surplus energy, and x is the confining pressure.

5. Analysis of Sandstone Damage Evolution under Unloading Conditions Based on Dissipated Energy

5.1. Definition of Damage Based on Dissipated Energy. Suppose that all of the energy input during the loading process of the rock is converted into elastic energy and dissipated energy. The elastic energy is recoverable, and the dissipated energy is mainly used for the damage and failure of the rock, and it is irreversible. During the entire unloading test, the damage process of the rock can also be considered as the result of the work done by the dissipated energy. The larger the dissipated energy, the greater the damage of the rock [38].

Kachanov defined the degree of damage using the changes of cross section, and its expression is [39] as follows:

$$D = \frac{A_0}{A}, \tag{14}$$

where A_0 is the total area of the micro-defects on the bearing section, and A is the section area when it is initially undamaged.

If the dissipated energy when the entire section A of the rock is completely damaged is U_{dmax}, then the dissipated energy U_{dw} required for the micro-element failure unit area is as follows:

$$U_{dw} = \frac{U_{dmax}}{A}. \tag{15}$$

The dissipated energy U_d required for the damage area to reach A_0 is as follows:

$$U_d = U_{dw}A_0 = \frac{U_{dmax}}{A}A_0. \tag{16}$$

In the test of triaxial unloading confining pressure, under the effect of the confining pressure, complete rock failure cannot be achieved, and there should be a certain residual strength; thus, the damage degree is generally less than 1. It is necessary to introduce a critical correction factor m; then, the calculation formula of damage variable is [40] as follows:

$$D = m\frac{U_d}{U_{dmax}},$$
$$m = 1 - \frac{\sigma_c}{\sigma_p}, \tag{17}$$

where σ_c is the residual strength of the rock sample, and σ_p is the peak strength of the rock sample.

5.2. Analysis of Damage Evolution Process. According to the above formula, the damage variable parameters of the yellow sandstone under unloading conditions with different confining pressures were calculated, and the normalization method was used to linearly transform the damage variable parameters. The calculation results are shown in Figure 13. It can be seen that the damage of the rock sample under each confining pressure at the initial loading stage slowly increases, and then the rock sample enters the elastic deformation stage and the damage level tends to be stable. The damage values of the rock sample after the unloading point all decrease, mainly because the reduction of confining pressure (σ_3) increases the deviator stress ($\sigma_1-\sigma_3$), so that the micro-cracks developed inside the rock sample are compressed and closed, leading to the decrease of the damage variable. Then, as the confining pressure continuously decreases, the damage variable continues to increase until the rock sample is completely damaged. The rising speed of the damage variable after the unloading point is significantly higher than the rising speed in the loading stage (where the loading speed is 2 MPa/min, and the unloading speed is 0.9 MPa/min), demonstrating that the rock damage caused by excavation unloading is more sudden than the loading
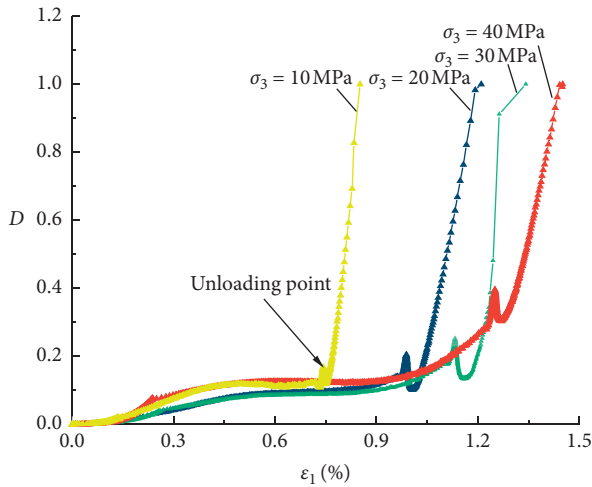
Figure 13: Damage evolution characteristics of sandstone unloading under different initial confining pressures.

failure. From the damage values at the unloading point, it can be seen that the higher the confining pressure, the larger the damage value, and the more obvious the upward trend of the damage variable before the unloading point. When the confining pressure increases from 10 MPa to 40 MPa by an increase of 10 MPa, the damage variable of the rock sample under different confining pressures is 1.24, 1.47, and 2.33 times greater than that under the confining pressure of 10 MPa, indicating that as the buried depth increases, the initial damage of the surrounding rock also intensifies, and excavation unloading is more prone to cause damage, making it more difficult to control the stability of the surrounding rock.

6. Conclusions

The failure process of the yellow sandstone under unloading conditions with different initial confining pressures was systematically studied. By analyzing the mechanical properties, energy conversion laws, and damage evolution characteristics, the following conclusions were obtained:

(1) The higher the initial confining pressure is, the faster will be the unloading instability of the rock sample falling to the residual strength; at the same time, with the rise of the confining pressure, both the dilatancy amount and the speed of the rock sample present a decreasing trend, and show the failure characteristics of dilatancy under low confining pressure and compression under high confining pressure. Before unloading to the critical point of failure, the higher the confining pressure, the greater the axial deformation; and in the whole unloading process, the higher the confining pressure, the smaller the radial deformation. The higher the initial confining pressure, the higher the confining pressure for the failure of the rock sample under unloading conditions, and there is a linear relationship; besides, the higher the

confining pressure, the greater the shear fracture energy required for the failure of the rock sample.

(2) Before the unloading point, almost all the energy absorbed by the rock under low initial confining pressure is converted into elastic energy, while a small part of the energy absorbed under high initial confining pressure is converted into dissipated energy. The higher the initial confining pressure, the greater the elastic energy, radial deformation energy, and dissipated energy at the rock fracture point.

(3) The higher the initial confining pressure, the greater the dissipated energy required for the failure of the rock sample under unloading conditions. In the compaction stage, the lower the confining pressure, the higher the proportion of dissipated energy; before the unloading point, the proportion of dissipated energy increases with the rising initial confining pressure, and the higher the confining pressure, the larger the proportion of dissipated energy at the unloading point.

(4) The higher the initial confining pressure, the greater the postpeak failure energy and surplus energy of the rock sample. The postpeak failure energy and surplus energy have a linear and quadratic polynomial relationship with the confining pressure, respectively, and the higher the confining pressure, the greater the proportion of elastic energy converted into surplus energy.

(5) The damage speed of the rock sample in the unloading stage is obviously higher than that in the loading stage, and the higher the confining pressure, the larger the damage value at the unloading point, indicating that the greater the buried depth, the larger the initial damage of the surrounding rock.

Data Availability

The data used to support the findings of this study are available from the corresponding author upon request.

Conflicts of Interest

The authors declare that they have no conflicts of interest.

Acknowledgments

with the fieldwork in Heilongjiang Ground Pressure and Gas Control in Deep Mining Key Lab (GPGC).

References

[1] G. Wu, J. Sun, and Z. R. Wu, "Damage mechanical analysis of unloading failure of intact rock mass under complex stress state," *Journal of Ho Hai University*, vol. 25, no. 3, pp. 44–49, 1997.

[2] S. G. Yu and L. J. Dong, "Statistics and analysis of academic publications for development of rock mechanics in China," *Chinese Journal of Rock Mechanics and Engineering*, vol. 32, no. 3, pp. 442–464, 2013.

[3] L. Wang, J. F Liu, H. T. Yang et al., "Experimental research on mechanical properties of deeply buried marble under unloading conditions," *Journal of Sichuan University (Engineering Science Edition)*, vol. 46, no. 2, pp. 46–51, 2014.

[4] X. F. GuoJ. M. Yin et al., "Mechanical property test at different unloading velocities of metamorphic quatz sandstone," *Journal of Shanghai Jiao Tong University*, vol. 50, no. 1, pp. 78–83, 2016.

[5] J. Li, F. Lin, H. Liu, and Z. Zhang, "Triaxial experimental study on changes in the mechanical properties of rocks under different rates of confining pressures unloading," *Soil Mechanics and Foundation Engineering*, vol. 56, no. 4, pp. 246–252, 2019.

[6] T. Wen, H. M. Tang, Z. Q. Fan et al., "Loading and unloading mechanical properties of rocks of Badong formation and its unloading constitutive model," *Journal of China University of Mining & Technology*, vol. 47, no. 4, pp. 768–779, 2018.

[7] Z. Y. Liu, M. S. Xiao, L. Zhuo et al., "Loading and unloading characteristics of mica-quartz schist and constitutive model for its unloading," *Chinese Journal of Geotechnical Engineering*, vol. 38, no. S2, pp. 85–91, 2016.

[8] J. Q. Guo, X. R. Liu, and Q. Zhao, "Theoretical research on rock unloading mechanical characteristics," *Rock and Soil Mechanics*, vol. 38, no. s2, pp. 123–130, 2017.

[9] J. L. Li, L. H. Wang, and X. S. Sun, "Experimental study on anisotropic mechanical characteristics of jointed rock masses under unloading condition," *Chinese Journal of Rock Mechanics and Engineering*, vol. 33, no. 5, pp. 892–900, 2014.

[10] G. Y. Duan, J. L. Li, J. Y. Zhang et al., "Mechanical properties and failure modes of rock specimens with specific joint geometries in triaxial unloading compressive test," *Advances in Materials Science and Engineering*, vol. 2019, 2019.

[11] Y. R. Yang, H. Q. Xie, M. L. Xiao et al., "Dilatancy and energy characteristics analysis of transverse-isotropic rock mass under triaxial unloading condition," *Rock and Soil Mechanics*, vol. 38, no. 6, pp. 1589–1599, 2017.

[12] Y. R. Yang, H. Q. Xie, M. L. Xiao et al., "Deformation failure and energy characteristics of transverse-isotropic rock under unloading of high confining pressure," *Chinese Journal of Rock Mechanics and Engineering*, vol. 36, no. 8, pp. 1999–2006, 2017.

[13] X. Z. Chen, J. D. He, M. L. Xiao et al., "Dilatancy and energy properties of marble under triaxial unloading condition," *Chinese Journal of Geotechnical Engineering*, vol. 36, no. 6, pp. 1106–1112, 2014.

[14] G. Y. Hou, J. P. Liang, H. Y. Jing et al., "Experimental study on deformation and acoustic emission characteristics of arch roadway under different unloading rates," *Advances in Civil Engineering*, vol. 2020, 2020.

[15] G. Y. Hou, J. P. Liang, H. Y. Jing et al., "Influence of deviatoric stress on the deformation and damage evolution of surrounding rock under unloading conditions," *Shock and Vibration*, vol. 2020, 2020.

[16] F. Xiao, D. Y. Jiang, F. Wu et al., "Effects of prior cyclic loading damage on failure characteristics of sandstone under true-triaxial unloading conditions," *International Journal of Rock Mechanics and Mining Sciences*, vol. 132, 2020.

[17] Q. H. Wu, X. B. Li, L. Weng et al., "Experimental investigation of the dynamic response of prestressed rockbolt by using an SHPB-based rockbolt test system," *Tunnelling and Underground Space Technology*, vol. 93, 2019.

[18] Q. H. Wu, L. Weng, Y. L. Zhao et al., "Deformation and cracking characteristics of ring-shaped granite with inclusion under diametrical compression," *Arabian Journal of Geosciences*, vol. 13, no. 14, 2020.

[19] J. Yu, G. F. Fu, X. Chen et al., "Experimental study on mechanical properties of sandstone after freezing-thawing cycles under triaxial confining pressure unloading," *Chinese Journal of Rock Mechanics and Engineering*, vol. 34, no. 10, pp. 2001–2009, 2015.

[20] X. H. Ni, X. M. Shen, and Z. D. Zhu, "Mechanical and acoustic emission characteristics of sandstone through triaxial unloading test after cyclic freezing-thawing treatment," *Advances in Civil Engineering*, vol. 2020, 2020.

[21] Y. Y. Cai, C. H. Luo, J. Yu et al., "Experimental study on mechanical properties of thermal-damage granite rock under triaxial unloading confining pressure," *Chinese Journal of Geotechnical Engineering*, vol. 37, no. 7, pp. 1173–1180, 2015.

[22] G. Q. Chen, T. B. Li, Y. H. He et al., "Thermo-mechanical coupling and rockburst tendency analysis of deep hard rock tunnel," *Chinese Journal of Rock Mechanics and Engineering*, vol. 32, no. 8, pp. 1554–1563, 2013.

[23] L. M. Qiu, Z. T. Liu, E. Y. Wang et al., "Early-warning of rock burst in coal mine by low-frequency electromagnetic radiation," *Engineering Geology*, vol. 279, 2020.

[24] L. M. Qiu, D. Z. Song, Z. H. Li, B. B. Liu, and J. Liu, "Research on AE and EMR response law of the driving face passing through the fault," *Safety Science*, vol. 117, pp. 184–193, 2019.

[25] L. M. Zhang, S. Gao, Z. Q. Wang et al., "Analysis of marble failure energy evolution under loading and unloading conditions," *Chinese Journal of Rock Mechanics and Engineering*, vol. 32, no. 8, pp. 1572–1578, 2013.

[26] Q. C. Fang, L. Shang, Y. H. Shang et al., "Mechanical and energy characteristics of granites under unloading test," *Journal of Central South University (Science and Technology)*, vol. 47, no. 12, pp. 4148–4153, 2016.

[27] D. Li, Z. Sun, T. Xie, X. Li, and P. G. Ranjith, "Energy evolution characteristics of hard rock during triaxial failure with different loading and unloading paths," *Engineering Geology*, vol. 228, pp. 270–281, 2017.

[28] W. L. Gong, X. Gao, Y. X. Sun et al., "Study on rock burst mechanisms based on dynamic Mohr's stress circle," *Chinese Journal of Rock Mechanics and Engineering*, vol. 38, no. S2, pp. 3321–3329, 2019.

[29] Z. Z. Zhang, M. Deng, J. B. Bai et al., "Strain energy evolution and conversion under triaxial unloading confining pressure tests due to gob-side entry retained," *International Journal of Rock Mechanics and Mining Sciences*, vol. 126, 2020.

[30] H. P. Xie, Y. Ju, and L. Y. Li, "Criteria for strength and structural failure of rocks based on energy dissipation and energy release principles," *Chinese Journal of Rock Mechanics and Engineering*, vol. 24, no. 17, pp. 3003–3010, 2005.

[31] B. Dai, G. Y. Zhao, C. Yang et al., "Criteria for strength and structural failure of rocks based on energy dissipation and

energy release principles," *Journal of Mining & Safety Engineering*, vol. 24, no. 17, pp. 3003–3010, 2005.

[32] G. Z. Yin, B. Ma, C. Liu et al., "Effect of loading and unloading rates on mechanical properties and energy characteristics of sandstone under true triaxial stress," *Journal of China Coal Society*, vol. 44, no. 2, pp. 454–462, 2019.

[33] Y. Chang, Z. Chen, F. Ren, and L. Chang, "Strain energy dissipation and damage evolution of frozen migmatite under triaxial unloading," *Geotechnical and Geological Engineering*, vol. 37, no. 4, pp. 3183–3192, 2019.

[34] G. Liu, Y. M. Li, F. K. Xiao et al., "Study on failure mechanics behavior and damage evolution law of yellow sandstone under uniaxial triaxial and pore water action," *Chinese Journal of Rock Mechanics and Engineering*, vol. 38, no. S2, pp. 3532–3544, 2019.

[35] S. G. Li, G. F. Chen, H. Q. Shuang et al., "Experimental study on effect of loading rate and initial damage on energy evolution of sandstone," *Journal of Mining & Safety Engineering*, vol. 36, no. 2, pp. 373–380, 2019.

[36] J. Ning, J. Wang, J. Jiang, S. Hu, L. Jiang, and X. Liu, "Estimation of crack initiation and propagation thresholds of confined brittle coal specimens based on energy dissipation theory," *Rock Mechanics and Rock Engineering*, vol. 51, no. 1, pp. 119–134, 2018.

[37] P. Liang, Y. B. Zhang, B. Z. Tian et al., "Experimental study on energy evolution characteristics in the process of tunnel rockbursts," *Chinese Journal of Rock Mechanics and Engineering*, vol. 38, no. 4, pp. 736–746, 2019.

[38] Y. J. Yang and D. P. Ma, "Experimental research on energy evolution properties of coal sample failure under triaxial unloading testing," *Journal of Mining & Safety Engineering*, vol. 35, no. 6, pp. 1208–1216, 2020.

[39] L. M. Kachanov, "Time rupture process under creep conditions," *Izvestia Akademii Nauk SSSR*, vol. 8, pp. 26–31, 1958.

[40] B. X. Liu, J. L. Huang, Z. Y. Wang et al., "Study on damage evolution and acoustic-emission character of coal-rock under uniaxial compression," *Chinese Journal of Rock Mechanics and Engineering*, vol. 28, no. S1, pp. 3234–3238, 2009.